

CFD study of an iterative focused wave generation method

Haoyuan Gu^{*1} and Hamn-Ching Chen²

¹Zachry Department of Civil and Environmental Engineering, Texas A&M University, College Station, TX, USA

²Zachry Department of Civil & Environmental Engineering and Ocean Engineering, Texas A&M University, College Station, TX, USA

(Received December 8, 2022, Revised February 2, 2023, Accepted February 5, 2023)

Abstract. An iterative focused wave generation method is developed and implemented in a local analytic based Navier-Stokes solver. This wave generation method is designed to reproduce the target focused wave by matching the target amplitude spectrum and phase angle. A 4-waves decomposition scheme is utilized to obtain the linearised component of the output wave. A model test studying the interaction between different focused waves and a fixed cylinder is selected as the target for the wave generation approach. The numerical wave elevations and dynamic pressure on the cylinder are compared with the experimental measurement and other state-of-the-art numerical methods' results. The overall results prove that the iterative adjustment method is able to optimize the focused wave generated by a CFD approach.

Keywords: computational fluid dynamics (CFD); extreme waves; focused wave generation

1. Introduction

Extreme wave, also known as rogue wave or freak wave, has been a significant problem for a long time due to its unpredictability and hazard (Kharif and Pelinovsky 2003, Dysthe *et al.* 2008). Compared to the moderate regular wave, extreme wave is highly nonlinear and often occurs transiently at an irregular and multi-frequency sea state. Although many catastrophic consequences have been caused by extreme wave according to observations in history, extreme wave's physical mechanism is still not robust (Dysthe *et al.* 2008).

To study the interactions between extreme waves and structures, it is of great importance to reproduce the target wave sequences in both experimental and numerical wave tanks. The most often used method is the dispersive focusing model, which determines the initial phase shifts of wave components based on wave's dispersion characteristics. Longuet-Higgins (1974) first utilized this model to generate groups of short large waves at a predefined location in a wave tank. Rapp and Melville (1990) investigated a breaking wave group under deep water condition based on this theory. The kinematics of the focused wave was further explored both experimentally (Baldock *et al.* 1996) and numerically (Baldock and Swan 1994). Tromans *et al.* (1991) developed the NewWave model to reproduce an extreme wave profile with a specified spectrum, which was later validated and widely used in coastal and ocean engineering areas (Jonathan and Taylor 1997, Bai and Taylor 2007, Christou and Ewans 2014).

*Corresponding author, Ph.D. Student, E-mail: hygu@tamu.edu

It should be noted that the dispersive focusing model is based on the linear wave theory. Due to the nonlinear wave-wave interaction, the generated focused wave is inevitably shifted in focus phase and position (Baldock *et al.* 1996). The focus shifting becomes more obvious for wave with high amplitude and narrow-banded spectrum, as the nonlinearity of the focused wave group is stronger. To solve this problem, Chaplin (1996) proposed an iterative procedure which repeatedly corrected each phase of the input wave component individually so that better phase distributions were generated at the predefined location. On the basis of this method, Schmittner *et al.* (2009) developed a phase-amplitude iteration scheme to generate more complex irregular wave sequences. Similar approach was implemented by Fernández *et al.* (2013) in a numerical wave tank with variable water depth. By using a harmonics separation technique, the focused wave spectrum was linearised and utilized in the iterative process experimentally (Buldakov *et al.* 2017) and numerically (Stagonas *et al.* 2018), which attempted to have a better control over the generated wave groups for steep waves.

Although linear and nonlinear potential flow theories have been commonly used in engineering practices of wave simulation, it may not be reliable enough to study the wave-structure interaction (WSI), especially under extreme wave condition. As the interaction between the extreme wave and structure is highly nonlinear, Computational Fluid Dynamics (CFD) method is a more competent solution to solve nonlinear problems such as wave breaking and air entrainment. Numerous CFD studies have been conducted to analyze interactions between different types of structures and extreme wave conditions, including floating wind turbine (Zhou *et al.* 2019), buoy (Bandringa *et al.* 2021), FPSO (Chen *et al.* 2019), etc. However, few studies have been conducted to improve the focused wave group by applying the iterative method in a CFD numerical wave tank. The iterative method proposed by Buldakov *et al.* (2017) was implemented in a CFD wave flume by matching the linearised target spectrum obtained from model test measurement (Stagonas *et al.* 2018, Higuera *et al.* 2018). The reason to use the linearised spectrum instead of the initial target spectrum of the physical experiment is to ensure the convergence and accuracy of the numerical wave generation. However, to obtain the linearised target spectrum from physical experiment, it is essential to generate waves with constant shifts for multiple times so that spectral decomposition technique can be applied for spectral separation. The process is time-consuming and may not be practical for every experimental condition. A more efficient and generic method is needed for the numerical wave generation to match the target wave spectrum from experimental measurement.

In this paper, an iterative focused wave generation method was implemented in an in-house CFD code based on the Finite-Analytic Navier-Stokes (FANS) method (Chen *et al.* 1990, Pontaza *et al.* 2005). This method was designed to reproduce a wide variety of non-breaking wave groups based on a target phase and amplitude spectrum. The focused waves measured at the model test by Sriram *et al.* (2015) were used as the target waves to validate the iterative approach. Both small and large amplitude wave cases were tested to evaluate the overall performance of this method. Description about the experimental setup is presented in Section 2. The numerical methodology is introduced in Section 3. The results are presented and discussed in Section 4. Conclusions are summarized in Section 5.

2. Experimental setup

A model test was designed to generate anticipated focused wave and then study the interaction between the focused wave and a fixed cylinder. The experiment was carried out in the wave tank at Ludwig Franzius Institute at Leibniz University of Hannover, Germany (Sriram *et al.* 2021a). A

Table 1 Wave packet characteristics

Case	f_c (Hz)	$\delta f/f_c$	f_i (Hz)	t_f (s)	N	G_a
1	0.68	1	0.34	38	32	0.001
3	0.68	1	0.34	38	32	0.003

Table 2 Wave probe locations

	Wave probe	X (m)	Y from sidewall (m)
X from wave maker	WP1	4.975	1.085 1.085
	WP2	13.928	
	WP3	14.178	1.085
	WP4	14.428	1.085
X from cylinder center	WP5	-0.570	0.825
	WP6	0.000	0.825
	WP7	0.705	0.825

Table 3 Pressure probe locations

Pressure probe	Vertical location (m)	Angular location (°)
PP1	0.415	0
PP2	0.515	0
PP3	0.615	0
PP4	0.715	0
PP5	0.815	0
PP6	0.615	20
PP7	0.615	90
PP8	0.615	180

constant steepness spectrum of 32 components was adopted for focused wave generation in the laboratory, with the help of a computer-controlled hydraulically driven piston type wave maker. Two focused waves of different amplitudes were generated based on second-order wave theory. The wave characteristics are presented in Table 1.

In the model test 7 wave probes were placed along the flume to measure the free surface elevation at a sampling rate of 100 Hz. A cylinder with a diameter of 0.22 m was fixed at the location where the wave developed to the target shape. Table 2 provides the locations of wave probes. 8 pressure sensors were mounted on the cylinder surface to measure the wave impact. Table 3 presents the locations of pressure probes. The experimental setup is shown in Figs. 1 and 2.

To apply the iterative focused wave method in the Navier-Stokes domain efficiently, the target focused wave at WP6 was first replicated by applying the iterative method in a 2D CFD numerical wave tank without the cylindrical pile. The adjusted input wave spectrum from the 2D simulation was further utilized as the incident wave spectrum in a 3D CFD model in order to study the wave impact on the cylinder.

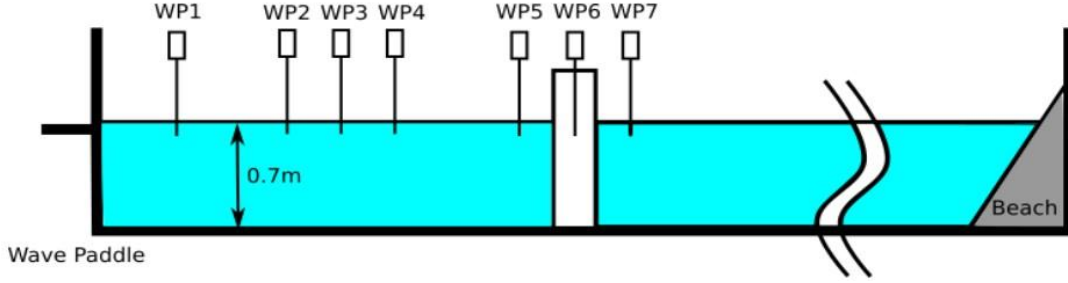


Fig. 1 Schematic of experimental setup (Sriram *et al.* 2021a)

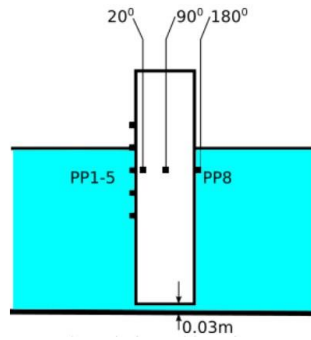


Fig. 2 Schematic of pressure probe locations (Sriram *et al.* 2021a)

3. Numerical methodologies and setup

3.1 Focused wave generation

The wave maker for the Navier-Stokes method was implemented by inputting the wave amplitude and velocity at the inlet boundary of the fluid domain. The free surface elevation, velocity and pressure were calculated analytically in a block based on the directional wave simulation (DWS) program by Huang and Zhang (2009). The analytical wave propagated from the DWS block to the neighboring FANS block through the overlapped region based on a structured overset grid system (Gu *et al.* 2019, Huang and Chen 2021). Details about the computational blocks are presented in Section 3.4. The wave free surface at the wave maker location in the DWS block is expressed in Eq. (1).

$$\eta(t) = \sum_{i=1}^N A_i \cos(\phi_i - \omega_i t) \quad (1)$$

where N is the total number of wave frequency components for the input wave spectrum, A_i is the wave amplitude of the i^{th} wave component, ω_i is the wave angular frequency, ϕ_i is the phase spectrum of the corresponding wave component. Both A_i and ϕ_i were obtained from the wave spectrum $S(\omega_i)$, which was transformed from the wave elevation time history based on Fourier Transform (FT). The location of WP2 in the model test was selected as the wave maker location, which means the initial input wave spectrum was based on the wave elevation time history measured at WP2.

Although the wave spectrum measured at WP2 was used as the initial input wave spectrum, it was not surprising to find that the numerical wave group developed at the focus location WP6 didn't match the experimental measurement. To solve this problem an iterative focused wave method was used in the numerical simulation. Both amplitudes and phases of the input wave components were adjusted iteratively until the desired focused wave was generated at the target location.

Assuming the nonlinear relationship between the input and output spectrum can be expanded in a series of Eq. (2), where $S(\omega)$ and $s(\omega)$ represent input and output wave amplitude spectrum in a form of complex functions. Based on the wave spectral decomposition method (Fitzgerald *et al.* 2014, Buldakov *et al.* 2017), the components of the amplitude spectrum can be separated with different orders of harmonics. In this paper a 4-waves decomposition scheme (Buldakov *et al.* 2017) was utilized. By linearly combining Eq. (2) with 4 constant input phase shifts $\Delta\phi = 0, \pi/2, \pi, 3\pi/2$, the sub-harmonics and super-harmonics for the first, second and third order terms were decomposed in Eq. (3).

$$s(\omega) = a_0 + a_1S(\omega) + a_2S(\omega)^2 + a_3S(\omega)^3 + \dots \quad (2)$$

$$\begin{aligned} S_0 &= \frac{s_0 + s_1 + s_2 + s_3}{4} \\ S_1 &= \frac{s_0 - is_1 - s_2 + is_3}{4} \\ S_2 &= \frac{s_0 - s_1 + s_2 - s_3}{4} \\ S_3 &= \frac{s_0 + is_1 - s_2 - is_3}{4} \end{aligned} \quad (3)$$

An iterative procedure in Eq. (4) was conducted to correct the input wave amplitude by comparing the output amplitude spectrum at the target location with the target spectrum.

$$a(\omega_i)_{in}^n = a(\omega_i)_{in}^{n-1} a(\omega_i)_{tgt} / a(\omega_i)_{out}^{n-1} \quad (4)$$

where $a(\omega_i)_{in}^n$ and $a(\omega_i)_{in}^{n-1}$ are the i^{th} frequency component's input amplitudes at n^{th} and $(n-1)^{th}$ iterations. $a(\omega_i)_{tgt}$ is the target amplitude spectrum of i^{th} frequency. $a(\omega_i)_{out}^{n-1}$ is the output amplitude at the $(n-1)^{th}$ iteration.

As the iterative procedure is only focused on the linearised amplitude correction, the nonlinear development of the wave propagation is not considered in this process. According to Buldakov *et al.* (2017), it is recommended to select the amplitude matching position in front of the phase focus location, so that nonlinear interaction can evolve naturally in the wave travelling process. This suggestion was also considered in the CFD simulation in this paper. The wave amplitude measured at WP4 was selected as the target wave amplitude in the iterative procedure of Eq. (4).

As for the procedure of phase correction, it has been proved by many previous studies such as Chaplin (1996) and Schmittner *et al.* (2009) that a direct comparison between the output wave phase angles and target wave phase angles works effectively to focus the wave at the target location. The iterative phase shift scheme is given below

$$\phi(\omega_i)_{in}^n = \phi(\omega_i)_{in}^{n-1} + [\phi(\omega_i)_{tgt} - \phi(\omega_i)_{out}^{n-1}] \quad (5)$$

where $\phi(\omega_i)_{in}^n$ and $\phi(\omega_i)_{in}^{n-1}$ are the i^{th} frequency component's input phase angles at n^{th} and $(n-1)^{th}$ iterations. $\phi(\omega_i)_{tgt}$ is the target phase angle of i^{th} frequency. $\phi(\omega_i)_{out}^{n-1}$ is the output phase angle at the $(n-1)^{th}$ iteration. The phase angle measured at WP6 was used as the target phase angle to ensure the desired focused wave at the phase focused location.

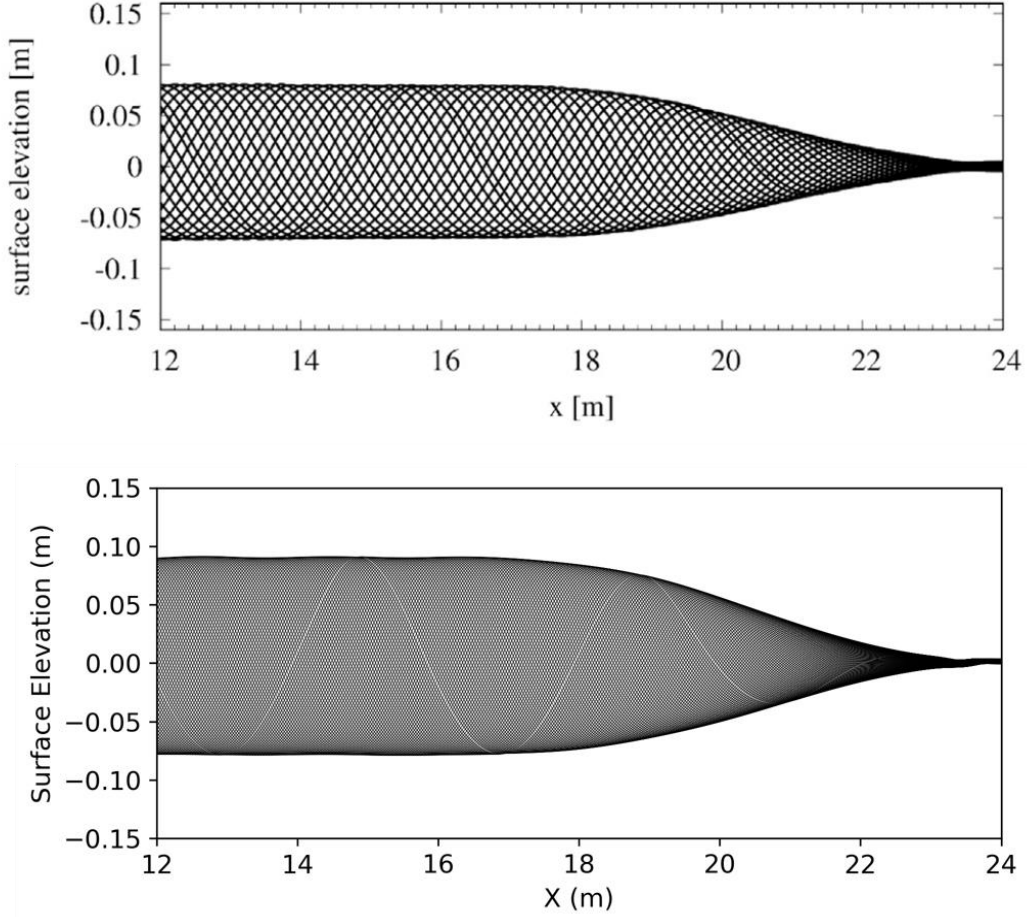


Fig. 3 Comparison of surface elevation in the vicinity of absorbing layer (upper: simulation result by Perić and Abdel-Maksoud (2018); lower: simulation result based on FANS)

3.2 Governing equation

Except for the analytical wave maker at WP2, the whole computational domain was based on the Finite-Analytic Navier-Stokes (FANS) numerical method developed by Chen *et al.* (1990) and Pontaza *et al.* (2005). The FANS method was programmed to solve unsteady and incompressible Navier-Stokes equations in general curvilinear coordinate systems.

To capture the wave free surface, an interface-capturing method based on the level set method (Osher and Sethian 1988) has been incorporated in the Navier-Stokes solver. Level set function ϕ separates air and water based on the definition in Eq. (6). In the transition zone where $|\phi| < \epsilon$, the fluid is smoothed by Heaviside function $H(\phi)$ in Eqs. (7) and (8).

$$\phi \begin{cases} > 0 & \text{water region} \\ = 0 & \text{air - water boundary} \\ < 0 & \text{air region} \end{cases} \quad (6)$$

$$H(\varphi) = \begin{cases} 0, & \varphi < -\epsilon \\ \frac{1}{2} \left(1 + \frac{\varphi}{\epsilon} + \frac{1}{\pi} \sin \left(\frac{\pi\varphi}{\epsilon} \right) \right), & -\epsilon \leq \varphi \leq \epsilon \\ 1, & \varphi > \epsilon \end{cases} \quad (7)$$

$$\begin{aligned} \rho(\varphi) &= \rho_a + (\rho_w - \rho_a)H(\varphi) \\ \mu(\varphi) &= \mu_a + (\mu_w - \mu_a)H(\varphi) \end{aligned} \quad (8)$$

The continuity and momentum equations in the level set formulation are then presented in Eqs. (9) and (10).

$$\sum_{i=1}^3 \frac{\partial U_i}{\partial x^i} = 0 \quad (9)$$

$$\frac{\partial U_i}{\partial t} + \sum_{j=1}^3 \left(U_j \frac{\partial U_i}{\partial x^j} + \frac{\partial u_i u_j}{\partial x^j} \right) + \frac{1}{\rho(\varphi)} \frac{\partial p}{\partial x^i} - \frac{\nu(\varphi)}{Re} \nabla^2 U_i + \frac{\delta_{i,3}}{Fr^2} = 0 \quad (10)$$

where U_i is the mean velocity component, u_i is the fluctuating velocity component, p is pressure, $\rho(\varphi)$ is non-dimensional fluid density, $\nu(\varphi) = \frac{\mu(\varphi)}{\rho(\varphi)}$ is the non-dimensional fluid viscosity, φ is the level-set function, $Re = \frac{\rho_w U_0 L}{\mu_w}$ is Reynolds number, $Fr = \frac{U_0}{\sqrt{gL}}$ is Froude number, $\delta_{i,j}$ is the Kronecker delta. The 3rd-order essentially non-oscillatory (ENO) scheme and total variation diminishing (TVD) Runge-Kutta scheme are used to discretize the level set equation (Yu 2007). The coupled method of FANS and level set model has been applied and validated in many previous studies, including green water (Chen and Yu 2009), nonlinear wave impact (Chen 2010) and wave-induced motion of a CALM buoy model (Huang *et al.* 2022).

3.3 Wave absorption

A forcing-zone type method was used to minimize the wave reflection at the end boundary of the Navier-Stokes domain. Absorbing source term of q_i was applied in the momentum equations in 3 directions. The formula of q_i inside the absorbing layer is presented in Eq. (11).

$$q_i = \gamma b(x)(u_{i,ref} - u_i) \quad (11)$$

where γ is the forcing strength, $b(x)$ is the blending function, $u_{i,ref}$ is the reference velocity and u_i is the velocity component. In this study an exponential blending function of $b(x) = \left[e^{\left(\frac{x-x_1}{x_2-x_1} \right)^2} - 1 \right] / (e - 1)$ was used. The absorbing layer thickness is $|x_2 - x_1|$, where x_1 is the beginning coordinate of absorbing layer, x_2 is the end coordinate of absorbing layer.

According to the analytical method by Perić and Abdel-Maksoud (2018), Perić and Abdel-Maksoud (2019), an optimal tuning of forcing strength γ can be achieved. The reflection coefficient C_R was introduced to evaluate the performance of the absorbing layer. The definition of the reflection coefficient for 1D regular wave train is presented in Eq. (12) according to Ursell *et al.* (1960).

$$C_R = \frac{|u_{max}| - |u_{min}|}{|u_{max}| + |u_{min}|} \quad (12)$$



Fig. 4 2D computational domain of Case 1

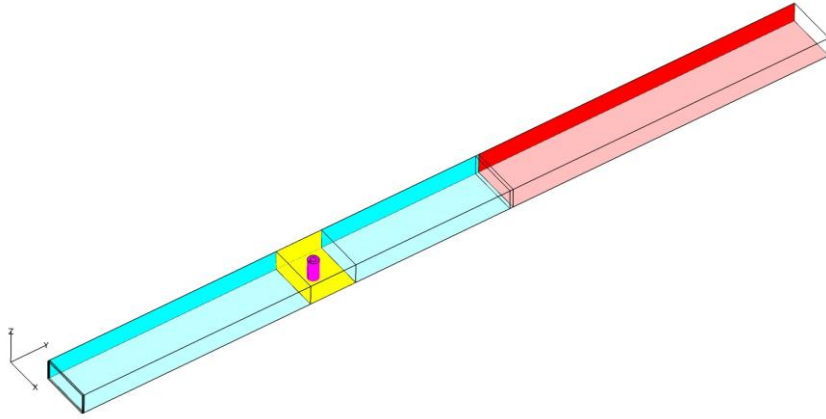


Fig. 5 3D computational domain of Case 1

where u_{max} and u_{min} are the maximum and minimum wave velocities at the location outside the absorbing layer during the last simulation period. The optimal forcing strength is obtained by looking for the minimum reflection coefficient.

To validate the application of the absorbing approach in the FANS method, a 1D regular wave test conducted in Perić and Abdel-Maksoud (2018) was replicated numerically. The regular wave height is $H = 0.16$ m. Period is $T = 1.6$ s. Wavelength is $\lambda \approx 4$ m. The forcing zone thickness is $x_d = 2\lambda$. The time step is $\Delta t = T/1000$. The total simulation time is $18s \approx 11.3T$.

Fig. 3 compares the numerical result by Perić and Abdel-Maksoud (2018) and the result simulated by the FANS solver with the same absorbing layer. The comparison shows a good agreement with the theoretical result, which means the analytical optimization method works well for the wave absorbing layer in the FANS domain.

3.4 Computational domain

Two focused wave cases conducted by Sriram *et al.* (2021a) were replicated numerically in the FANS domain. Two CFD models were prepared for each focused wave case. The first CFD model was a 2D wave basin model without a cylinder, with three stations of cells in transverse direction. Considering the transverse grid distribution, there is no change of the numerical wave in the crossflow direction. The iterative focused wave generation approach in Section 3.1 was utilized in the first model. The adjusted input wave based on the iterative method was used as the incident wave for the second CFD model, which was a 3D wave basin model with a cylinder.

Fig. 4 shows the 2D computational domain for Case 1. The domain is composed of three rectangular blocks based on a structured overset grid system. The black block was placed at the wave

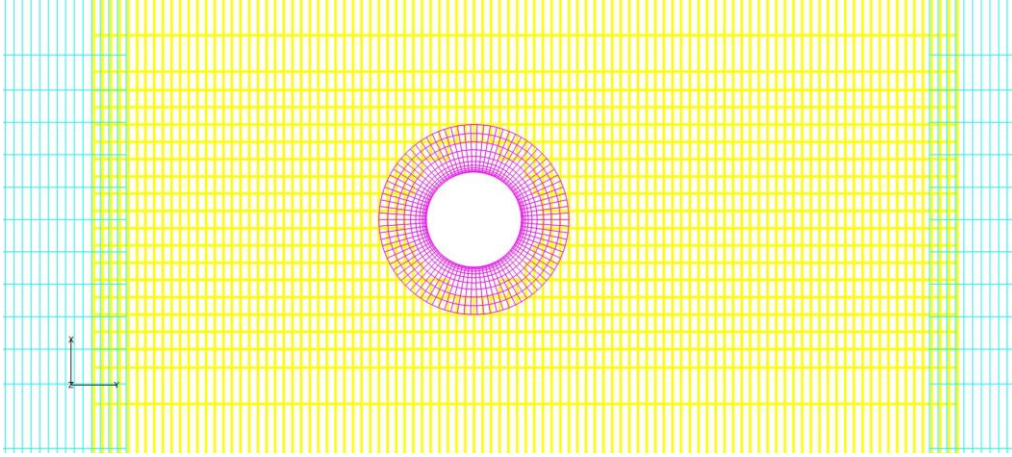


Fig. 6 Close-up view of grids around the cylindrical model

maker (WP2) location. It is an analytical DWS block with grid nodes of $3 \times 10 \times 73$. The wave velocities and elevations were interpolated on the boundary of the cyan Navier-Stokes domain based on the PEGSUS program (Suhs and Tramel 1991). The dimension of the Navier-Stokes domain is about $2.2 \text{ m} \times 33.0 \text{ m} \times 0.9 \text{ m}$. The end red region of the computational domain is the wave absorbing beach, which is $2\lambda_p \approx 14.14\text{m}$. λ_p is the wave length of the peak wave period T_p .

Fig. 5 displays the computational domain of the 3D model for Case 1. The size of the numerical wave basin is the same as the 2D model. A cylindrical model was built at the designed location of the experiment. The cylindrical model was surrounded by a self-overlapped O-type grid in the circumferential direction. Fig. 6 displays the top view of the detailed overset grid system near the cylinder. To better capture the interaction between the wave and the cylinder, a finer rectangular mesh was created in the vicinity of cylinder. There are 26 layers of grids in the transverse direction. In the outer fluid domain, the number of cells reduces to 17 in the transverse direction. The minimum grid size in longitudinal direction is 0.02 m . The grid surrounding the cylinder ranges from 0.002 m to 0.02m in the radial direction. The minimum vertical spacing is 0.0025 m in free surface region.

The structure of the computational domain for Case 2 is similar to the model for Case 1. The dimension of the wave basin is about $2.2 \text{ m} \times 33.0 \text{ m} \times 1.4 \text{ m}$. The minimum grid spacing in the longitudinal directions is 0.02 m . The minimum grid spacing in the vertical direction is 0.005 m . The horizontal grid distribution of the cylindrical model for Case 2 is the same as the grid distribution for Case 1. In both cases, the CFL condition is satisfied with $C_0 < 1$.

4. Results

4.1 Spectral analysis of iterative method

The output of the iterative focused wave method is displayed in Fig. 7, which compares the linearised spectrum and phase angles of each frequency mode before/after the iterative adjustment. As discussed in Section 3.1, the input wave is adjusted iteratively so that the linearised amplitude

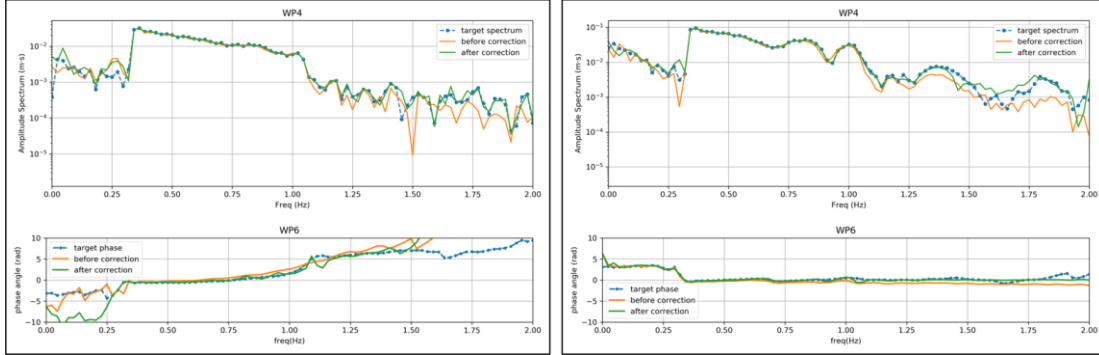


Fig. 7 Linearised spectrum and phases at target locations (left: small amplitude Case 1; right: large amplitude Case 2)

spectrum at WP4 and the output phase angle at WP6 are converged to the target spectrum and phase angle. The left subplots show the comparison for the small amplitude case. The right subplots show the comparison for the large amplitude case. For both cases a better agreement of the linearised amplitude spectrum at WP4 is achieved after the iterative procedure. It is obvious that the sub-harmonics ($0 < f < 0.34 \text{ Hz}$) and super-harmonics ($1.02 < f < 2.04 \text{ Hz}$) components are better captured after the correction. The phases within the primary range ($0.34 \leq f \leq 1.02 \text{ Hz}$) are better focused to the target phases at WP6. However the phases of sub-harmonics and super-harmonics are shifted for the small amplitude case. One of the reasons, according to Sriram *et al.* (2021b), is due to the difficulty in capturing the small amplitude of wave packets in numerical simulation.

It should be noted that the iteration numbers for convergence are different for cases with different amplitudes. For the small amplitude case three iterations were conducted to converge to a desired focus wave. For the large amplitude case the numerical result converges to the target result within four iterations. Within each iteration four parallel cases were conducted with four constant phase shifts (Section 3.1). Each case of 44s was computed with one core in a Dell x86 HPC Cluster. For the small amplitude case, a 2D mesh of 315,000 cells took 7.5 hours to complete an iteration. For the large amplitude case with 415,000 cells, it took about 10 hours to finish an iteration.

4.2 Wave elevation analysis

The time series results of wave elevations at WP5, WP6 and WP7 are presented in Fig. 8 for small amplitude case and Fig. 9 for large amplitude case. In comparison to the output wave before the correction, the wave after the correction is more focused in phase. The crest and trough of the focused wave are both improved after the iteration. For small amplitude case, the numerical wave after the highest crest agrees well with the physical target wave elevation. However for large amplitude case, the method fails to capture the high-frequency wave oscillation after the highest crest passes the focus location. One of the reasons is that the nonlinear wave-wave interaction during the wave propagation induces the energy transfer from lower to higher frequency components. As the linear wave amplitude spectrum is adjusted based on target wave measured at WP4, which is far from the focus position at WP6, it is difficult to fully control the super-harmonics components developed in the wave transmission process. The uncontrollable nonlinear interaction also contributes to the discrepancy between the numerical and experimental highest wave crest.

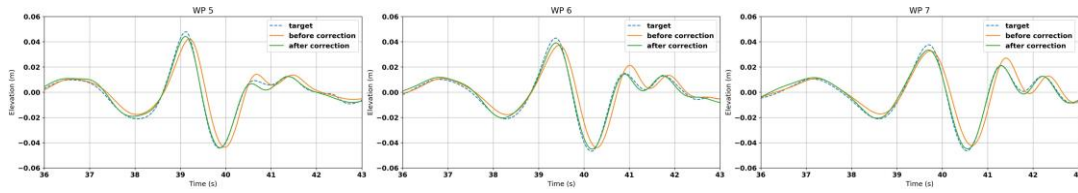


Fig. 8 Wave elevation time series for small amplitude case

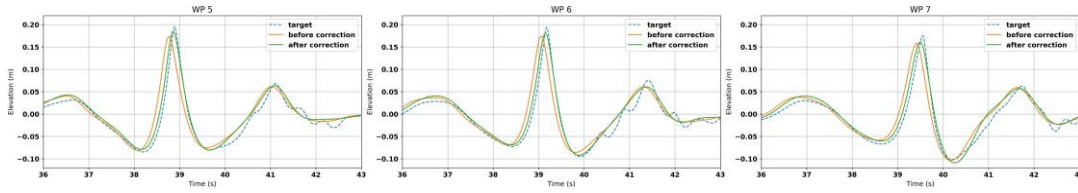


Fig. 9 Wave elevation time series for large amplitude case

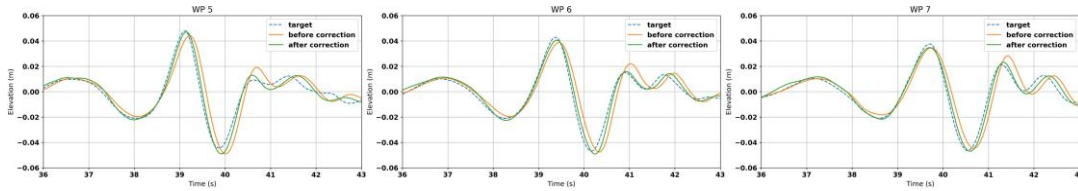


Fig. 10 Comparison of wave elevation time series for small amplitude case in 3D CFD model

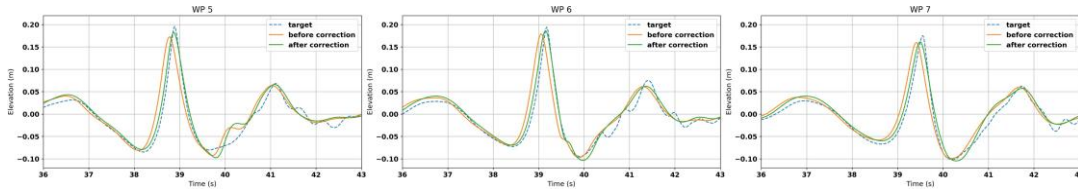


Fig. 11 Comparison of wave elevation time series for large amplitude case in 3D CFD model

The corrected input wave from the iterative method was further applied as the incident wave condition for the 3D CFD simulation with a cylindrical model. Figs. 10 and 11 present the time history of wave elevations in the 3D model for both cases. Compared to the wave elevation time series based on the initial input wave, the adjusted focused wave agrees better with the target wave. It is noted that compared to the 2D simulation, the 3D simulation has a higher crest and lower trough, which is obvious before and after the peak wave. Another discrepancy is that for the time series at WP5 in Fig. 11, a free surface oscillation occurred at the trough location when the simulation time was around 40s. This phenomenon is not observed in the 2D simulation and experimental measurement. Based on the 3D view of free surface elevation in the bottom two subplots of Fig. 13, it is deduced that the oscillation comes from the diffraction of cylinder.

To better illustrate the change of wave elevation in the vicinity of cylinder near the focused time, Figs. 12 and 13 present the 3D views of the free surface in the vicinity of the cylinder. For small amplitude case, the free surface is slightly disturbed on the leeward side of the cylinder. For large amplitude case, the free surface wraps around the cylinder and generates obvious run-up in the

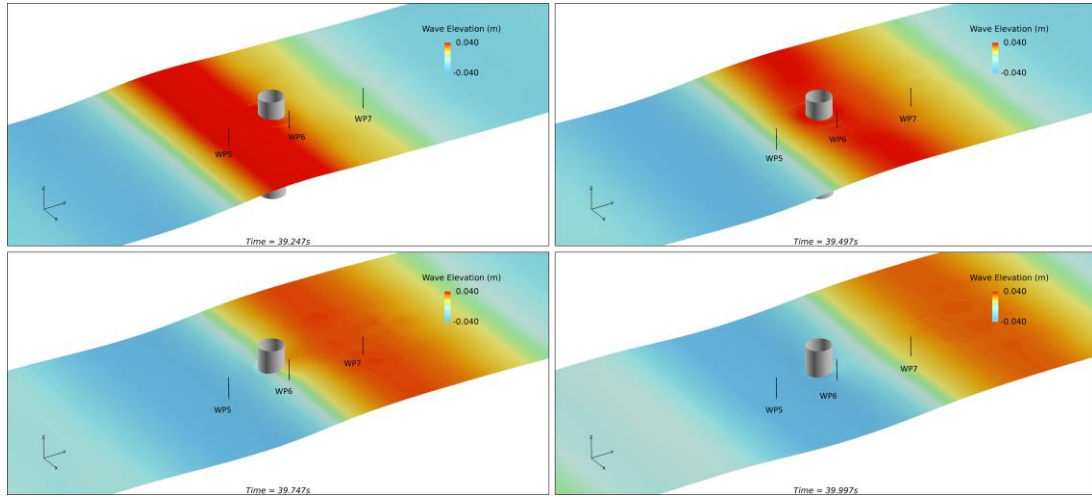


Fig. 12 3D view of wave elevation for small amplitude case

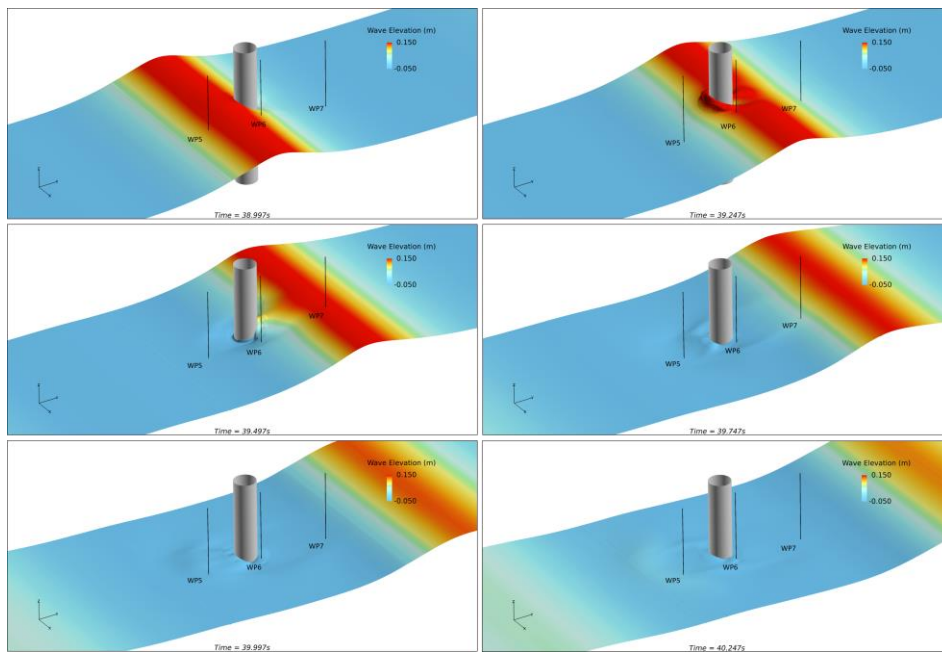


Fig. 13 3D view of wave elevation for large amplitude case

nearby region. The diffraction of the flow by the cylinder is observed to affect the wave elevation at WP5 and WP6.

Many other state-of-the-art numerical solvers also conducted the numerical simulation based on this model test. Their results were presented and compared by Sriram *et al.* (2021b). The majority of the numerical methods combined a potential flow model in the far field and Navier-Stokes model near the cylinder. Some other numerical models, such as full Navier-Stokes domain model (like the model used in this paper) and full potential flow domain model, were also employed and compared

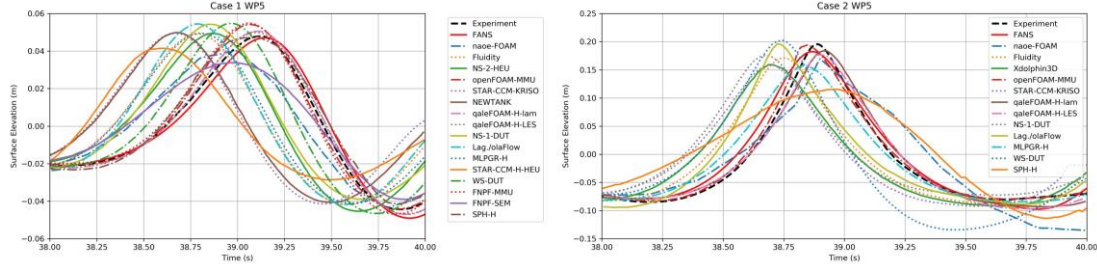


Fig. 14 Comparison of all numerical wave elevation time series

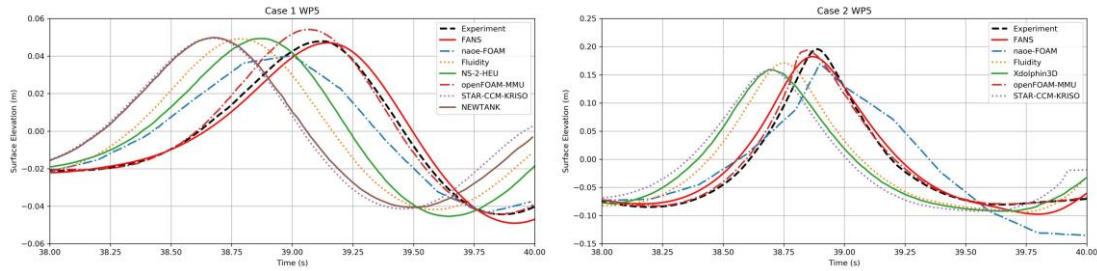


Fig. 15 Comparison of wave elevation time series in full Navier-Stokes domain

in the study. In order to have an overall assessment of the iterative method, the 3D numerical results are compared to other simulation results summarized in the comparative study.

The left subplot in Fig. 14 compares the wave elevation time history at WP5 for small amplitude case. The right subplot compares the wave elevation time history at the same location for large amplitude case. The comparison shows that the FANS result is one of the best numerical results with good agreement to the experimental measurement. It should be noted that most of the results in the comparative study were obtained based on a hybrid method. For example, the qaleFOAM solver by Yan *et al.* (2020) utilized a potential theory (FNPT) to simulate the outer fluid domain. The Navier-Stokes model was only applied in a small region surrounding the cylinder with a radius of 1.1m. Without the effect of viscous dissipation and numerical damping, the hybrid method keeps a close match of target wave before the numerical wave enters the inlet boundary of the Navier-Stokes domain. The effect of Navier-Stokes model on the wave development during the transmission process is weakened due to the limited size of Navier-Stokes domain.

To better evaluate the effect of iterative method on the Navier-Stokes domain, the wave elevation results which were solely solved by Navier-Stokes equation are extracted and analyzed in Fig. 15. With no correction method applied in the focused wave generation, most of the results in the full Navier-Stokes domain have evident discrepancies from the target wave, in both crest height and phase focus. Based on the comparison of the FANS simulation results before and after the correction method, it is implied that the iterative wave correction method also works for other numerical solvers.

4.3 Wave impact analysis

A comparative study of the wave impact pressure on the cylinder is presented in this section. The time series results of dynamic pressure at pressure probes are presented in Fig. 16 for small

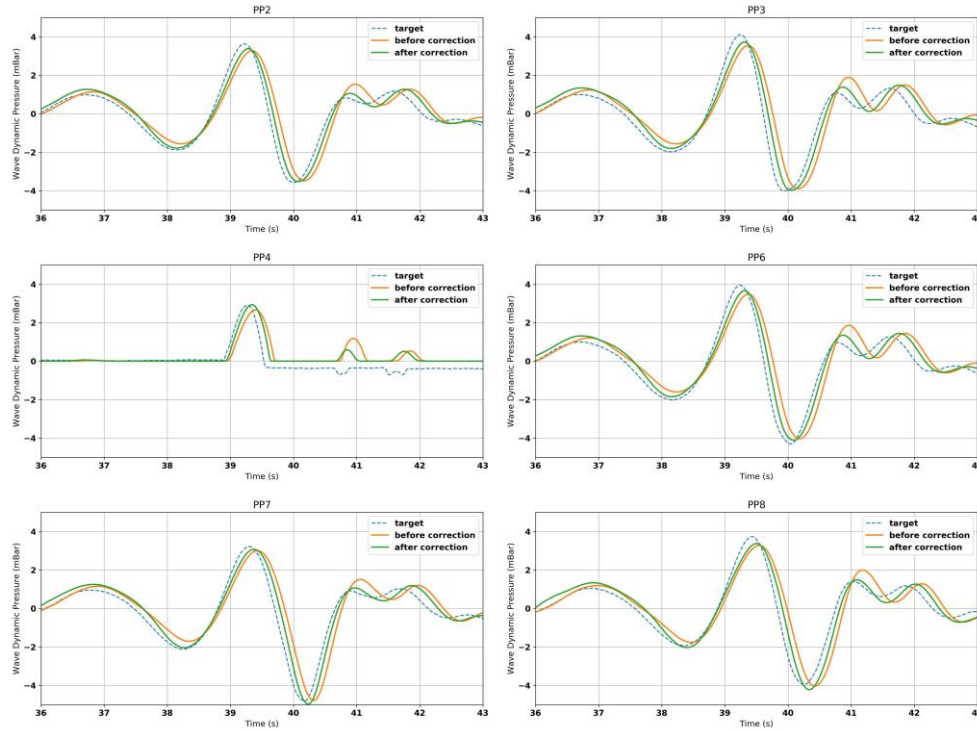


Fig. 16 Comparison of wave pressure time series for small amplitude case

amplitude case and Fig. 17 for large amplitude case. Compared to the numerical results before the correction, the overall results after the correction are improved at the wave focused time. It should be noted that in Fig. 16 the dynamic pressure measured at PP4 is negative after the crest surpasses the cylinder. This phenomenon is not captured by the numerical simulation. As the probe PP4 is located above the still water level, theoretically PP4 is no longer affected by the wave after the crest surpasses the cylinder. The negative measurement may be due to the experimental error in the model test, e.g., the water left on the pressure sensor.

The dynamic pressure comparisons of all the numerical simulation results are presented in Fig. 18 for small amplitude case and Fig. 19 for large amplitude case. For small amplitude case, the peak wave pressure is about 0.1s later than the experimental data, which is consistent with the small phase shift of wave elevation at WP6 in Fig. 10.

Figs. 20 and 21 compare the focused wave impact solved by the full domain of Navier Stokes equation. It should be noted that for both cases at PP4, none of the numerical solver successfully captures the dynamic pressure change at the tail of the crest. For the large amplitude case, the measured pressure shows a short jump before returning to zero. For small amplitude case, the measured pressure drops to a negative value starting from $t \approx 39.5s$.

In general the overall numerical pressure agrees well with the experimental measurement for both cases. To better analyze the effect of focused wave on the dynamic pressure, the side views of pressure distribution on the cylinder are presented in Figs. 22 and 23 for both cases. The snapshots are taken at the moments when the focused wave surpasses the cylinder. The distribution of dynamic pressure on the cylinder is strongly affected by the focused wave.

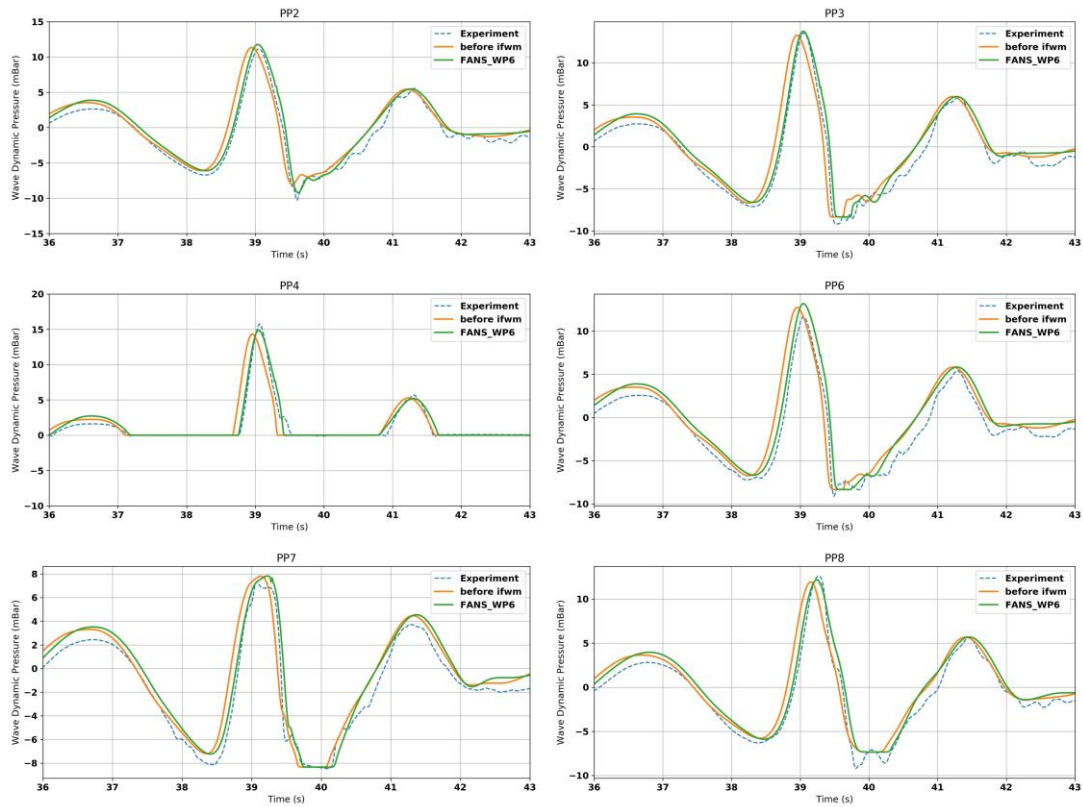


Fig. 17 Comparison of wave pressure time series for large amplitude case

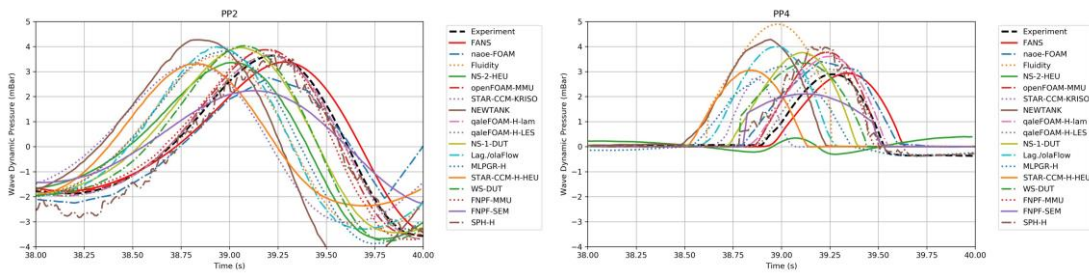


Fig. 18 Comparison of all numerical wave pressure time series for small amplitude case

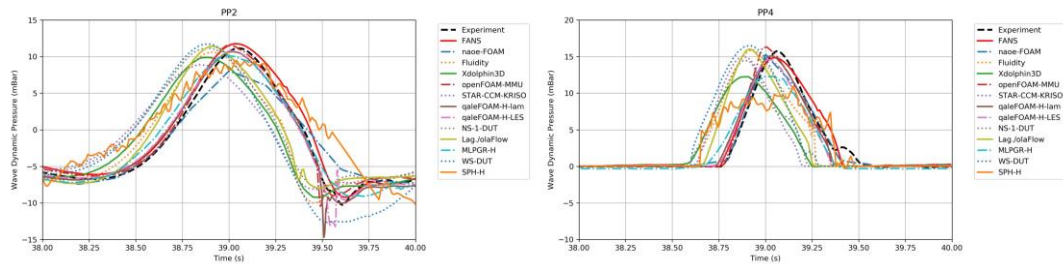


Fig. 19 Comparison of all numerical wave pressure time series for large amplitude case

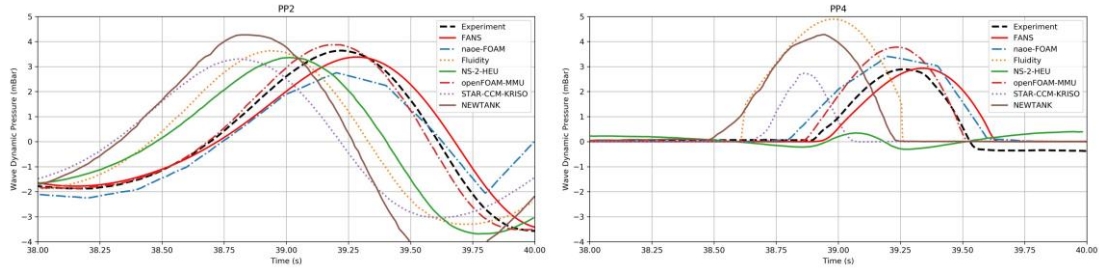


Fig. 20 Comparison of wave dynamic pressure in full Navier-Stokes domain for small amplitude case

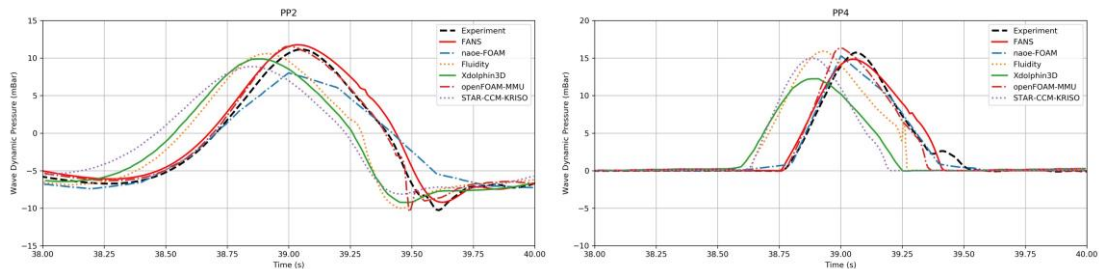


Fig. 21 Comparison of wave dynamic pressure in full Navier-Stokes domain for large amplitude case

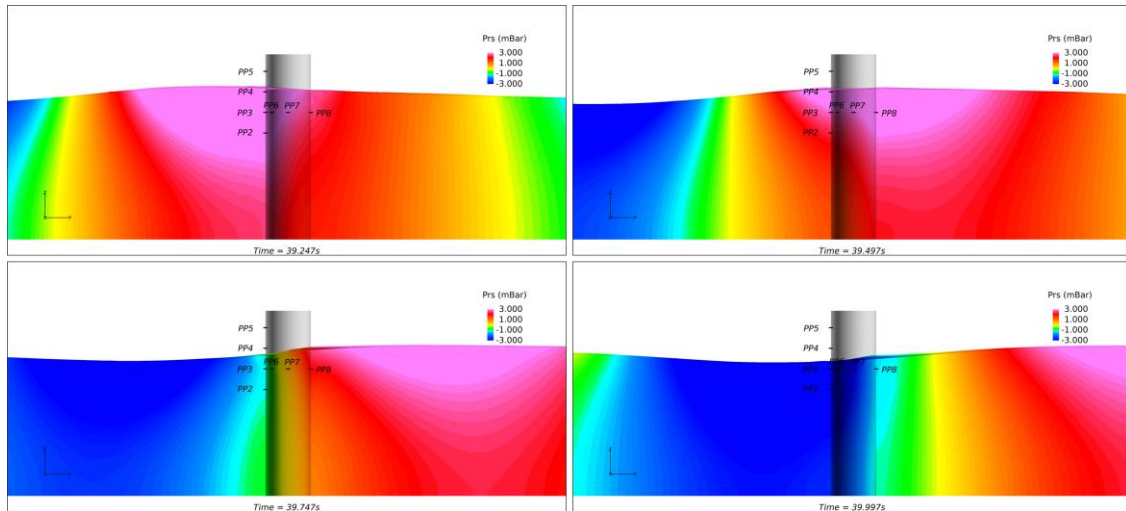


Fig. 22 2D wave dynamic pressure for small amplitude case

5. Conclusions

In this paper an iterative focused wave generation method was applied and studied in a Navier-Stokes solver named Finite-Analytic Navier-Stokes (FANS). The focused wave elevation measured at a model test was used as the target wave to evaluate the method. The model test was designed to study the interaction between the focused wave and a fixed cylinder. To evaluate the capability of the iterative method, both test cases with different focused wave amplitudes were studied. A 4-waves

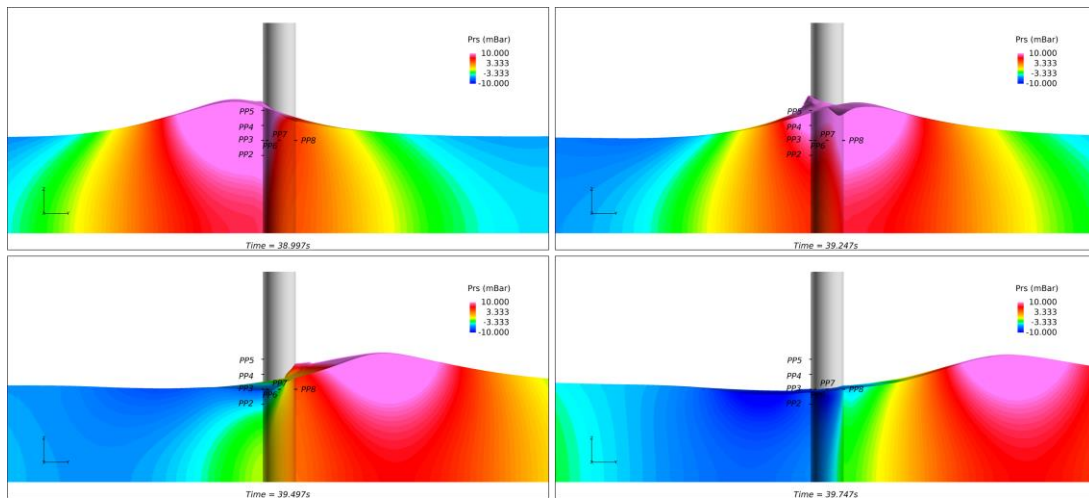


Fig. 23 2D wave dynamic pressure for large amplitude case

decomposition scheme was utilized to get the linearised component of the output wave spectrum, which means for each correction step 4 parallel numerical simulations were conducted with 4 constant input phase shifts. To reduce the influence of wave nonlinearity on the linearised amplitude matching, the amplitude matching location was selected in front of the phase focused location. The number of iterations mainly depends on the nonlinearity of the target wave spectrum. Larger focused wave amplitude tends to require more iteration steps to achieve equivalent performance as smaller wave amplitude case.

The iterative correction method was applied in the 2D model for efficient repetition of focused wave generation. Compared to the 3D model, the 2D model has less cells in the crossflow direction. The cylindrical model is also omitted in the 2D model under the assumption that the influence of cylinder on the measured wave elevation is negligible.

The corrected input wave based on the 2D model was utilized as the incident wave condition for the 3D model with cylinder. The numerical wave elevation and dynamic pressure detected in the 3D model are compared with the experimental data and other numerical methods' results for validation and evaluation.

The comparison of wave elevations before and after the correction proves the effectiveness of the iterative adjustment method. Although the numerical wave generated based on initial incident wave condition shows a similar profile to the target focused wave elevation, the wave after the adjustment has a better agreement with the target, in both wave amplitude and phase focus. It should be noted that based on the current method it is still unable to capture the super-harmonics components for highly nonlinear spectrum. The high-frequency free surface oscillation after the highest crest is not captured for the large amplitude case. The capability of this iterative correction method is further proved by comparing with numerical results from other solvers. As this method is not limited to the type of wave maker and numerical solver, it is anticipated that the prediction by other numerical method will be more accurate by applying the correction procedure.

In addition to the wave elevation measured at the wave probes, the fluid dynamic pressure on the cylinder is also investigated. The result shows that the FANS solver is able to provide reliable wave impact load on the structure. Due to the improved estimation of the focused wave crest after the

correction procedure, the wave impact load above the still water level is successfully captured. Based on the focused wave generation method that has been developed so far, further investigation will be conducted to study the hydrodynamic responses of floating structures under focused wave condition.

Acknowledgements

The authors would like to appreciate the computing resources supported by the High Performance Research Computing (HPRC) Center, Texas A&M University. The authors are particularly grateful to Dr. Buldakov and Dr. Stagonas for their kind and patient guidance in the wave spectral decomposition method.

References

- Bai, W. and Taylor, R.E. (2007), “Numerical simulation of fully nonlinear regular and focused wave diffraction around a vertical cylinder using domain decomposition”, *Appl. Ocean Res.*, **29**(1-2), 55-71. <https://doi.org/10.1016/j.apor.2007.05.005>.
- Baldock, T. and Swan, C. (1994), “Numerical calculations of large transient water waves”, *Appl. Ocean Res.*, **16**(2), 101-112. [https://doi.org/10.1016/0141-1187\(94\)90006-X](https://doi.org/10.1016/0141-1187(94)90006-X).
- Baldock, T., Swan, C. and Taylor, P. (1996), “A laboratory study of nonlinear surface waves on water”, *Philos. T. R. Soc. A*, **354**(1707), 649-676. <https://doi.org/10.1098/rsta.1996.0022>.
- Bandringa, H., Jaouën, F., Helder, J. and Bunnik, T. (2021), “On the validity of CFD for simulating a shallow water CALM buoy in extreme waves”, *Proceedings of the International Conference on Offshore Mechanics and Arctic Engineering*, volume 85116, page V001T01A037, American Society of Mechanical Engineers.
- Buldakov, E., Stagonas, D. and Simons, R. (2017), “Extreme wave groups in a wave flume: Controlled generation and breaking onset”, *Coast. Eng.*, **128**, 75-83. <https://doi.org/10.1016/j.coastaleng.2017.08.003>.
- Chaplin, J.R. (1996), “On frequency-focusing unidirectional waves”, *Int. J. Offshore Polar Eng.*, **6**(2).
- Chen, H., Qian, L., Bai, W., Ma, Z., Lin, Z. and Xue, M.A. (2019), “Oblique focused wave group generation and interaction with a fixed FPSO-shaped body: 3D CFD simulations and comparison with experiments”, *Ocean Eng.*, **192**, 106524. <https://doi.org/10.1016/j.oceaneng.2019.106524>.
- Chen, H.C. (2010), “Time-domain simulation of nonlinear wave impact loads on fixed offshore platform and decks”, *Int. J. Offshore Polar*, **20**(4).
- Chen, H.C., Patel, V.C. and Ju, S. (1990), “Solutions of Reynolds-averaged Navier-Stokes equations for three-dimensional incompressible flows”, *J. Comput. Phys.*, **88**(2), 305-336. [https://doi.org/10.1016/0021-9991\(90\)90182-Z](https://doi.org/10.1016/0021-9991(90)90182-Z).
- Chen, H.C. and Yu, K. (2009), “CFD simulations of wave-current-body interactions including greenwater and wet deck slamming”, *Comput. Fluids*, **38**(5), 970-980. <https://doi.org/10.1016/j.compfluid.2008.01.026>.
- Christou, M. and Ewans, K. (2014), “Field measurements of rogue water waves”, *J. Phys. Oceanogr.*, **44**(9), 2317-2335. <https://doi.org/10.1175/JPO-D-13-0199.1>.
- Dysthe, K., Krogstad, H.E. and Müller, P. (2008), “Oceanic rogue waves”, *Annu. Rev. Fluid Mech.*, **40**, 287-310. <https://doi.org/10.1146/annurev.fluid.40.111406.102203>.
- Fernández, H., Schimmels, S. and Sriram, V. (2013), “Focused wave generation by means of a self correcting method”, *Proceedings of the 23rd International Offshore and Polar Engineering Conference*, OnePetro.
- Fitzgerald, C., Taylor, P.H., Taylor, R.E., Grice, J. and Zang, J. (2014), “Phase manipulation and the harmonic components of ringing forces on a surface-piercing column”, *P. R. Soc. A: Math. Phys.*, **470**(2168), 20130847. <https://doi.org/10.1098/rspa.2013.0847>.
- Gu, H., Chen, H.C. and Zhao, L. (2019), “Coupled CFD-FEM simulation of hydrodynamic responses of a CALM buoy”, *Ocean. Syst. Eng.*, **9**(1), 21-42. <https://doi.org/10.12989/ose.2019.9.1.021>

- Higuera, P., Buldakov, E. and Stagonas, D. (2018), “Numerical modelling of wave interaction with an FPSO using a combination of OpenFOAM R and lagrangian models”, *Proceedings of the 28th International Ocean and Polar Engineering Conference*, OnePetro.
- Huang, H. and Chen, H.C. (2021), “Coupled CFD-FEM simulation for the wave-induced motion of a CALM buoy with waves modeled by a level-set approach”, *Appl. Ocean Res.*, **110**, 102584. <https://doi.org/10.1016/j.apor.2021.102584>.
- Huang, H., Gu, H. and Chen, H.C. (2022), “A new method to couple FEM mooring program with CFD to simulate Six-DoF responses of a moored body”, *Ocean Eng.*, **250**, 110944. <https://doi.org/10.1016/j.oceaneng.2022.110944>.
- Huang, L. and Zhang, J. (2009), Introduction to Program DWS (Directional Wave Simulation), Technical report, Technical Report, Ocean Engineering Program, Texas A&M University, College.
- Jonathan, P. and Taylor, P.H. (1997), “On irregular, nonlinear waves in a spread sea”, *Offshore Mech. Arct. Eng.*, **119**(1), 37-41. <https://doi.org/10.1115/1.2829043>.
- Kharif, C. and Pelinovsky, E. (2003), “Physical mechanisms of the rogue wave phenomenon”, *Eur. J. Mech.-B/Fluids*, **22**(6), 603-634. <https://doi.org/10.1016/j.euromechflu.2003.09.002>.
- Longuet-Higgins, M. (1974), “Breaking waves in deep or shallow water”, *Proceedings of the 10th Conf. on Naval Hydrodynamics*, MIT.
- Osher, S. and Sethian, J.A. (1988), “Fronts propagating with curvature-dependent speed: Algorithms based on Hamilton-Jacobi formulations”, *J. Comput. Phys.*, **79**(1), 12-49. [https://doi.org/10.1016/0021-9991\(88\)90002-2](https://doi.org/10.1016/0021-9991(88)90002-2).
- Perić, R. and Abdel-Maksoud, M. (2018), “Analytical prediction of reflection coefficients for wave absorbing layers in flow simulations of regular free-surface waves”, *Ocean Eng.*, **147**, 132-147. <https://doi.org/10.1016/j.oceaneng.2017.10.009>.
- Peric, R. and Abdel-Maksoud, M. (2019), “Damping of non-linear and irregular long-crested freesurface waves using forcing zones”, *Proceedings of the 11th International Workshop on Ship and Marine Hydrodynamics (IWSH2019)*.
- Pontaza, J., Chen, H. and Reddy, J. (2005), “A local-analytic-based discretization procedure for the numerical solution of incompressible flows”, *Int. J. Numer. Meth. Fl.*, **49**(6), 657-699. <https://doi.org/10.1002/fld.1005>.
- Rapp, R.J. and Melville, W.K. (1990), “Laboratory measurements of deep-water breaking waves”, *Philos. T. R. Soc. A*, **331**(1622), 735-800. <https://doi.org/10.1098/rsta.1990.0098>.
- Schmittner, C., Kosleck, S. and Hennig, J. (2009), “A phase-amplitude iteration scheme for the optimization of deterministic wave sequences”, *Proceedings of the International Conference on Offshore Mechanics and Arctic Engineering*.
- Sriram, V., Agarwal, S. and Schlurmann, T. (2021a), “Laboratory study on steep wave Interactions with fixed and moving cylinder”, *Int. J. Offshore Polar*, **31**(1), 19-26. <https://doi.org/10.17736/ijope.2021.jc808>.
- Sriram, V., Agarwal, S., Yan, S., Xie, Z., Saincher, S., Schlurmann, T., Ma, Q., Stoesser, T., Zhuang, Y., Han, B. *et al.* (2021b), “A comparative study on the nonlinear interaction between a focusing wave and cylinder using state-of-the-art solvers: Part A”, *Int. J. Offshore Polar*, **31**(1), 1-10. <https://doi.org/10.17736/ijope.2021.jc820>.
- Sriram, V., Schlurmann, T. and Schimmels, S. (2015), “Focused wave evolution using linear and second order wavemaker theory”, *Appl. Ocean Res.*, **53**, 279-296. <https://doi.org/10.1016/j.apor.2015.09.007>.
- Stagonas, D., Higuera, P. and Buldakov, E. (2018), “Simulating breaking focused waves in CFD: Methodology for controlled generation of first and second order”, *J. Waterway Port C. ASCE*, **144**(2). [https://doi.org/10.1061/\(ASCE\)WW.1943-5460.0000420](https://doi.org/10.1061/(ASCE)WW.1943-5460.0000420).
- Suhs, N. and Tramel, R. (1991), PEGSUS 4.0 user’s manual, Technical report, Arnold Engineering Development Center Arnold AFB TN.
- Tromans, P.S., Anaturk, A.R. and Hagemeyer, P. (1991), “A new model for the kinematics of large ocean waves-application as a design wave”, *Proceedings of the 1st international offshore and polar engineering conference*, OnePetro.
- Ursell, F., Dean, R.G. and Yu, Y. (1960), “Forced small-amplitude water waves: a comparison of theory and experiment”, *J. Fluid Mech.*, **7**(1), 33-52. <https://doi.org/10.1017/S0022112060000037>.

- Yan, S., Ma, Q., Asnim, W., Sulaiman, Z. and Sun, H. (2020), “Comparative study on focusing wave interaction with cylinder using QALE-FEM and qaleFOAM”, *Proceedings of the 30th International Ocean and Polar Engineering Conference*, OnePetro.
- Yu, K. (2007), Level-set RANS method for sloshing and green water simulations, Texas A&M University.
- Zhou, Y., Xiao, Q., Liu, Y., Incecik, A., Peyrard, C., Li, S. and Pan, G. (2019), “Numerical modelling of dynamic responses of a floating offshore wind turbine subject to focused waves”, *Energies*, **12**(18), 3482. <https://doi.org/10.3390/en12183482>.

MK